

High Resolution Z-Contrast Imaging of Semiconductor Interfaces

D.E. Jesson and S.J. Pennycook

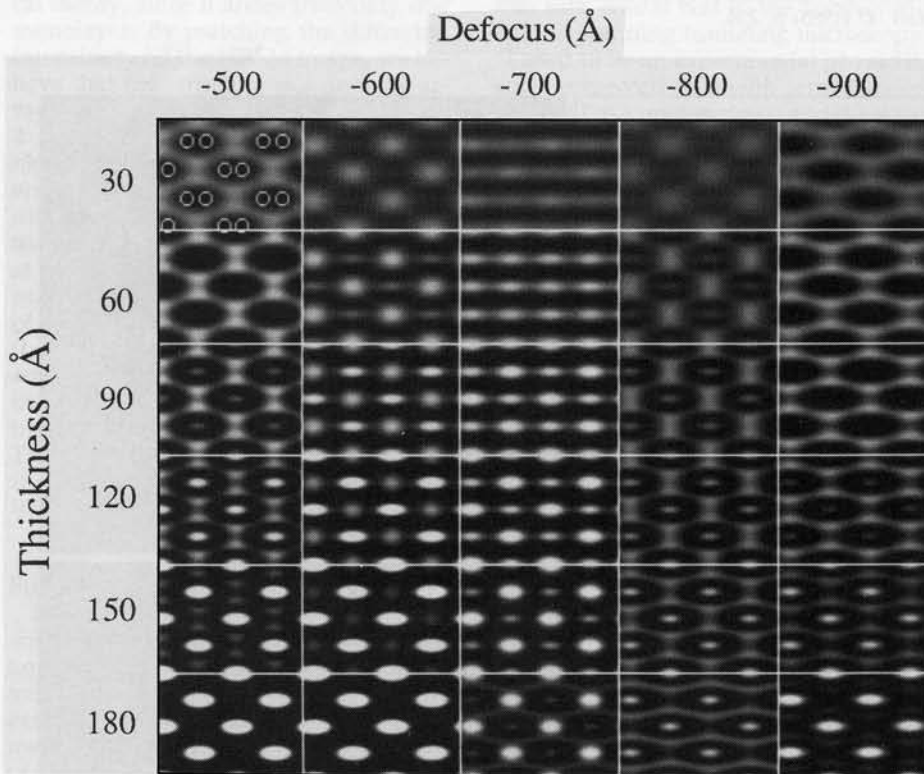


Figure 1. Montage of phase contrast simulated images for Si $\langle 110 \rangle$. The accelerating voltage is 400 keV, and the objective lens spherical aberration coefficient C_s is 1 mm (Scherzer resolution limit 1.7 Å).

Introduction

The structural and compositional integrity of interfaces between semiconductor multilayers can profoundly influence the optical and electronic properties of

epitaxially grown heterostructures. Understanding the atomic-scale interfacial structure and chemistry is therefore essential to correctly relate electrical measurements to theoretical models and to

correlate such effects with growth conditions. High-resolution electron microscopy (HREM) has played a pivotal role in this process, providing important information on interface commensurability and revealing the presence and nature of defects.

More recently, significant advances have been made in applying HREM to the difficult problem of chemical composition mapping in systems where no structural change occurs across the interfaces.¹ The basis of such methods involves using the objective lens as a bandpass filter and tuning in on a specific range of spatial frequencies to form a chemically sensitive interference pattern. By using a suitable low-index zone axis and choosing an optimum range of specimen thickness, the patterns can indeed be extremely sensitive to the strength and periodicities of the projected potential.

However, the results also depend critically on other experimental parameters including small specimen tilts and strains. It is customary to establish the optimum experimental chemical mapping conditions from a sequence of image simulations based on the anticipated structure and chemistry of the system under investigation. This type of pretuning may, however, reduce the sensitivity of the interference pattern to unforeseen structural effects, which might easily be overlooked in the image.

This article presents a new strategy for compositional mapping at semiconductor interfaces, using Z-contrast scanning transmission electron microscopy (STEM). Our approach is to incoherently image an interface object function which is intuitively related to the structure and chemistry of the interface. Images exhibit a weak thickness dependence and a strong (Z^2) chemical sensitivity. No pretuning of the experimental conditions is required since the instrument is operated at standard defocus conditions for all specimens. This direct method provides the crystal grower with immediate feedback on the atomic-scale structure and chemistry of the heterostructure, and most importantly, rapidly identifies unexpected effects. We illustrate these points through experimental studies of ultrathin $(\text{Si}_m\text{Ge}_n)_p$ superlattices and CoSi_2/Si interfaces which demonstrate the unique insights the technique can provide into the atomistic processes occurring during epitaxial growth.

How to Think About Z-Contrast Images

Z-contrast STEM imaging is funda-

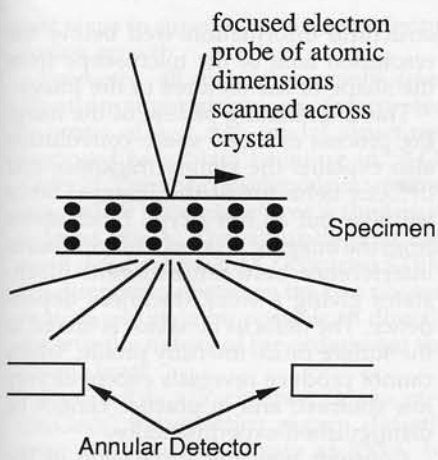


Figure 2. Formation of a Z-contrast image in the STEM from Rutherford scattered electrons.

mentally different from conventional HREM imaging methods. Conventional HREM is a coherent imaging process in which the image is reconstructed from a set of diffracted beams (see the article by J.M. Gibson in this issue). The phases of these beams are sensitive to objective lens defocus and specimen thickness so that the image can take many forms (Figure 1). In Z-contrast STEM, however, we scan a small (~ 2.2 Å FWHM) coherent electron probe across the surface of a thin specimen (Figure 2). Simultaneously, we detect transmitted electrons scattered through high angles using an annular detector with a large inner angle. The image is then built up sequentially as a function of probe position as, for example, in scanning tunneling microscopy (STM). The images we obtain display surprisingly strong incoherent characteristics, even in relatively thick specimens (~ 500 Å). Images simply blur with defocus, rather like a camera, and possess a weak thickness dependence exhibiting no reversals. The simulated through-focus sequence displayed in Figure 3 exhibits just one optimum contrast condition at -700 Å. Either side of this condition, the image starts to wash out and gradually fades away. There are no contrast reversals so that atomic columns are unambiguously identified as bright spots in the image. The thickness dependence of the image is equally straightforward as shown in Figure 4. The image always retains the same form, gradually increasing in intensity as more scatterers contribute to each column, although eventually losing contrast as the probe

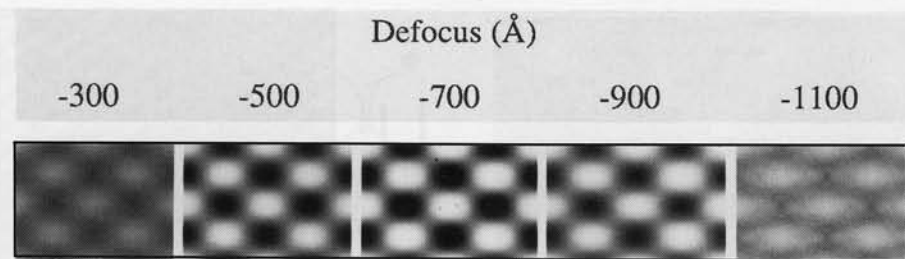


Figure 3. Simulated Z-contrast defocus series for Si$\langle 110 \rangle$ using 100 keV accelerating voltage and an objective lens C_s of 1.3 mm (Scherzer resolution limit 2.2 Å).

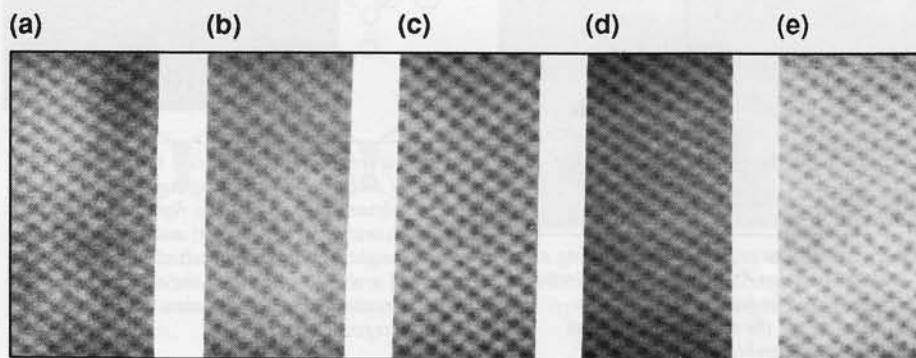


Figure 4. Z-contrast images from Si$\langle 110 \rangle$ obtained at: (a) 120, (b) 230, (c) 350, (d) 470, and (e) 610 Å, respectively.

current is reduced close to the atomic sites by absorption.

At first sight, the reason why we obtain incoherent images at atomic resolution is not at all obvious. After all, we focus a coherent electron probe at the entrance surface of the crystal which then diffracts strongly as it propagates along the zone axis direction. To see how the incoherent characteristics arise is best achieved using a Bloch-wave description of the dynamical probe propagation, and we refer you to several recent papers that cover this topic in detail.^{2,5} Our aim in this article is to provide a simple prescription for how one should think about and interpret Z-contrast images of interfaces. This conveys why the imaging is both intuitive and immediately suggestive of the structure and chemistry of the interface.

In a typical Z-contrast experiment, we utilize the most compact probe condition⁴ and tilt the crystal to a low index zone-axis where the atoms project into well-separated strings or columns. The relevant Si[110] projection is sketched in Figure 5a, for example, and consists of

closely spaced pairs of atoms or dumbbells. In the Z-contrast case, we do not image the projected potential but needles of scattering power located at each column position as shown in Figure 5b. This is because the high-angle scattering originates very close to the atom sites. The width of the needles is on the order of the rms thermal vibration amplitude which for Si at room temperature is ~ 0.1 Å.⁴ It is important to note that the array of needles in Figure 5b accurately maps the projected atom positions, i.e., it acts as a structural fingerprint for the crystal projection. The compositional information is contained in the weighting of the needles. This is simply the sum of scattering power to high angles of the individual atoms contained within the column multiplied by the thickness integrated probe wavefunction intensity close to the atom sites.

To evaluate the probe wavefunction intensity at the atom sites would at first sight seem to require a supercomputer. However, the insight provided by Bloch-wave methods shows how the coherent electron probe combined with a high-

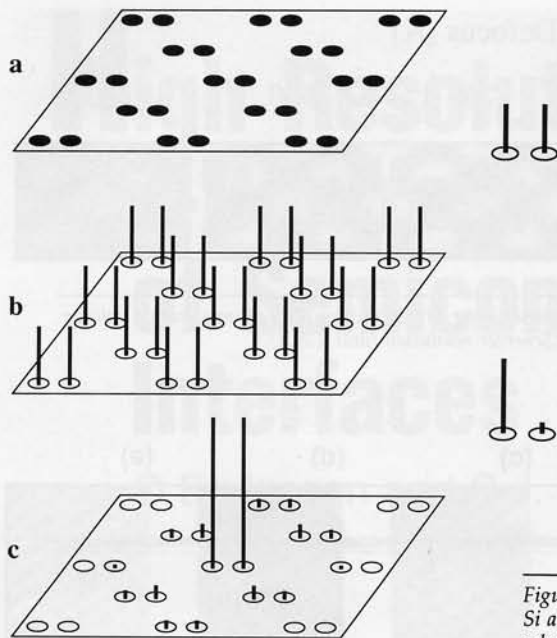


Figure 5. The process of constructing an object function for the Si(110) projection represented in (a). In (b), we place "needles" at the projected atom sites which are weighted by the effective scattering power of each column. In (c), we represent the image formation process with the probe located over the central dumbbell by weighting the object in (b) with the surface probe intensity profile. An incoherent sum over the resultant needles then gives the Z-contrast image intensity.

angle detector affords a tremendous simplification. In essence, we have a filtering effect of the Bloch-states (the stationary states of a fast electron in the crystal). Only one type of Bloch-state (s-type) contributes to the imaging, and the thickness integration becomes a simple analytical expression.

It turns out that the weighting of the needles is dominated by the high-angle atomic cross sections which are highly sensitive to composition, approaching the atomic number squared or Z^2 dependence of unscreened Rutherford scattering. Thus, we arrive at the real space object shown in Figure 5b. The object function is not the crystal potential, rather, it is a simple, compositionally sensitive map which efficiently characterizes the projection. The positions of the needles map the column positions, and the needle heights map the scattering power of the columns. This is the object we image incoherently in

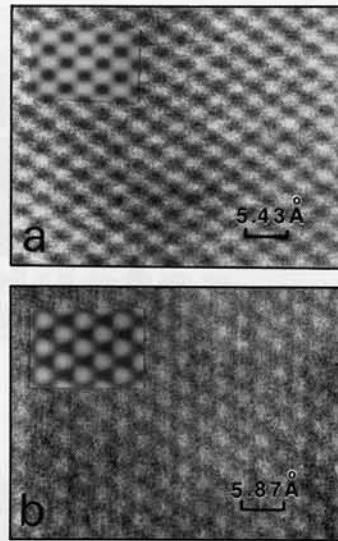


Figure 6. $\langle 110 \rangle$ Z-contrast images of (a) Si and (b) InP with cross sections of the relevant object functions representing the atomic dumbbells. Equal and unequal weightings of the unresolved needles for Si and InP give rise to the elongated and circular features in the simulated (inset) images, respectively.

Z-contrast STEM. To generate the image intensity for a probe at any position on the object, we simply weight the array of needles with the envelope of the surface probe intensity profile. This is illustrated in Figure 5c with the probe located over the central dumbbell. A sum over all of the scattering power needles then gives the Z-contrast image intensity for that probe position. Mathematically, this is simply a convolution of the surface probe intensity profile with the object function and is rather straightforward to visualize.

Consider, for example, the Z-contrast images of Si and InP in Figure 6. For the Si[110] projection, the bright spots in the image are elongated, rather like "rugby balls," due to the close proximity of the pairs of unresolved needles representing the dumbbells (Figure 6a). For InP, however, the dumbbells are comprised of nonequivalent In and P columns so that the corresponding object function consists of unequal strength needles with the In needle dominating the convolution (Figure 6b). Consequently, the image consists of rather circular bright features ("soccer balls") as expected. Thus, from the simple form of the object function and probe intensity profile, it is quite possible to deduce interpretable

structural information well below the resolution limit of the microscope from the shape of the features in the image.

This illuminating picture of the imaging process as a real space convolution also explains the simple thickness and defocus behavior of the images. Since we filter out all but s-type Bloch-states from the imaging process, this precludes interference between different Bloch-states giving a weak thickness dependence. The defocus behavior is linked to the surface probe intensity profile, which cannot produce reversals except at very low contrast, and in practice cannot be distinguished experimentally.

Consider now the application of the object function description of Z-contrast imaging to the case of interfaces. The fact that the scattering needles are weighted by highly localized s-states means that each needle is essentially independent of its neighbors. This breaks down (as for Si $\langle 110 \rangle$) when the columns are so close that the s-states overlap, and the relevant molecular orbital state should be used to weight the needles. In either case, interface object functions may be assembled column-by-column, which is the reason Z-contrast images of interfaces may be interpreted intuitively or simulated quantitatively on a small computer.

The following section will illustrate this intuitive imaging capability, which is the most important advantage of the Z-contrast technique. All images are obtained under identical experimental conditions. The probe shape is the same for every specimen, so there is no need to tune the microscope conditions based on a preknowledge of the crystal structure. In this way, one can truly allow the materials microstructure to provide the surprises, and indeed we do find surprises, even in systems studied for many years using many different techniques.

Intuitive Imaging of Semiconductor Interfaces

In our first example, we will look at the very topical case of ultrathin (Si_mGe_n)_p superlattices grown by MBE. The aim is to produce a direct band-gap material by flipping the band structure at the Brillouin zone boundaries. However, all the relevant band-structure calculations assume abrupt interfaces, which is perhaps significant in the light of recent diffraction evidence for interfacial ordering in the Si-Ge system.⁶ Therefore, it is important to determine the origin, structure, and morphology of the ordering, both to explain the electrooptical behavior of ultrathin superlattices and to sug-

gest ways to suppress or avoid ordering during growth.

Presently, all diffraction results from ultrathin superlattices are interpreted in terms of just two model structures proposed to explain ordering in Si-Ge alloys.⁷⁻⁹ There is considerable interest as to which of these structures is the "true" ordered phase. The simulations in Figure 7 clearly show that Z-contrast STEM can discriminate between the two phases, so it should now be possible to directly observe the nature of the ordering at the atomic level.

Figure 8 is a Z-contrast image of a $(\text{Si}_4\text{Ge}_8)_{24}$ superlattice grown directly onto a Ge(001) substrate at 350°C by molecular beam epitaxy (MBE).¹¹ The bright horizontal bands represent the deposited Ge layers (stronger scattering power), and the darker bands are the deposited Si layers. Remarkably, we observe three distinct types of ordering within the deposited Si layers. In the top Si layer, there is a strong $(2 \times n)$ periodicity, in the central layer alternate $\langle 111 \rangle$ planar ordering, and in the bottom Si layer, crosslike structures. We also observe an asymmetric interfacial abruptness in our images, that is, the Si grown on Ge interface is less abrupt than the Ge grown on Si interface. The simple idea of a single-ordered phase is, therefore, totally inappropriate for the low-temperature growth of superlattices. A different ordered structure can occur at each interface and would be impossible to deduce from selected area diffraction which would average over all of the phases.

The information contained in Figure 8, therefore, represents a valuable opportunity to understand the atomistic processes occurring during the growth of ultrathin Si-Ge multilayers. Indeed, the $(2 \times n)$ periodicities contained within the Si layers strongly imply that the ordering is in some way linked to Si deposition on the Ge free surface, which is known to possess a (2×1) reconstruction.¹² We assume that growth occurs via monolayer-height island formation and the consecutive interchange of (1×2) and (2×1) domains by analogy with Si(001) homoepitaxy (see the article by Robert J. Hamers in this issue). At low temperatures, this process is strongly anisotropic with a preferred growth direction perpendicular to the dimer rows of the original (2×1) reconstruction. Growth, therefore, occurs via single-layer type S_B steps in the notation of Chadi.¹³ This process is represented schematically in Figure 9, where we consider in cross section the growth of a narrow

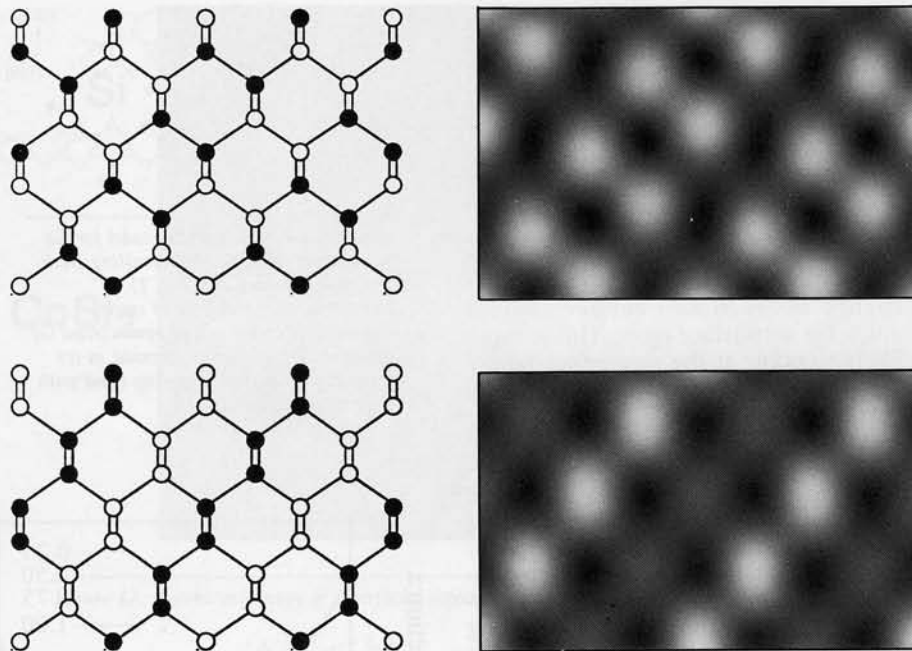


Figure 7. Z-contrast simulations of the two model structures proposed by Ourmazd and Bean⁷ for ordering in the Si-Ge system. Open circles represent Ge columns and solid circles Si columns.

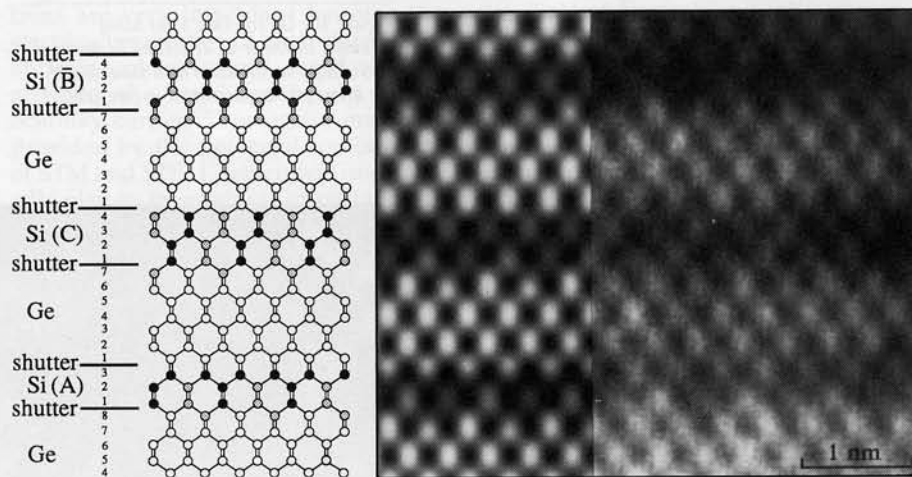


Figure 8. [110] Z-contrast STEM image of a nominal $(\text{Si}_4\text{Ge}_8)_{24}$ superlattice showing interfacial ordering. The [001] growth surface is toward the top of the image. Our interpretation of the superlattice structure based on the image simulation indicates the sequential deposition of Si and Ge layers together with ordered structures B, C, and A (see Reference 10) resulting from the atom pump mechanism. Solid circles represent Si columns, open circles Ge columns, and shaded circles alloy columns. A convergence angle of 10.3 mrad, objective lens C_s of 1.3 mm, and defocus of -70 nm was assumed in the simulations.

island (or single dimer string) along $[1\bar{1}0]$.

Since the Ge surface has a (2×1) reconstruction, the growth is forced through two distinct types of S_B steps. It is well known that a Ge-reconstructed surface has a lower surface energy than the corresponding Si (2×1) surface, primarily because of the difference in surface dangling bond energies. It, therefore, makes sense to look for possible candidate sites involving an interchange between a Si surface adatom and a Ge subsurface atom. This is more likely to occur at the step edges where the atoms are weakly bound and possess higher mobilities.

In the nonrebonded edge configuration (Figure 9b), an interchange of a surface Si edge atom with the Ge edge atom will conserve the number of dangling bonds and is energetically unfavorable. However, the rebonded edge step configuration (Figure 9c) now allows the possibility of burying a surface Si dangling bond and replacing it with a more stable Ge surface dangling bond (Figure 9d). We estimate an energy gain of 0.45 eV per exchange so that the rebonded edge step acts as a chemically driven atom pump for Ge segregation.¹⁰ Since the growth is forced sequentially through the stable-unstable configurations, this asymmetric pumping mechanism configures the dimer string(s) into alternating Si and Si-Ge alloy columns as growth proceeds along $[1\bar{1}0]$. Thus, compositional ordering can be attributed to surface growth dynamics.

Since each island appears to nucleate independently, coalescence into larger islands will be accompanied by the formation of antiphase boundaries between translationally inequivalent (2×1) domains. The intrinsically small domain size associated with low-temperature epitaxy will also restrict the lateral extent of the ordered domains which is in excellent agreement with our observations. Carrying the model through shows that many different phase variants are possible depending on the direction of step propagation and precisely how the preceding layers have grown in the superlattice.¹⁰ Ordering may propagate, terminate, or reverse during each successive monolayer growth step. Furthermore, each structure must also exhibit ordering along the orthogonal $[110]$ direction and possess a compositional modulation in the $[001]$ growth direction, reflecting a decay in Ge concentration away from the interface.

We can see clearly that the actual situation is much more complicated than previously supposed. The original ques-

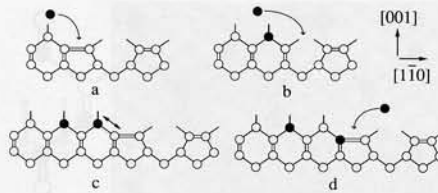


Figure 9. Growth kinetics model for Ge segregation and ordering resulting from Si deposition on a Ge (2×1) reconstructed surface. Solid circles represent Si columns and open circles Ge columns. The exchange arrowed in (c) replaces a Si surface dangling bond with a Ge dangling bond (d).

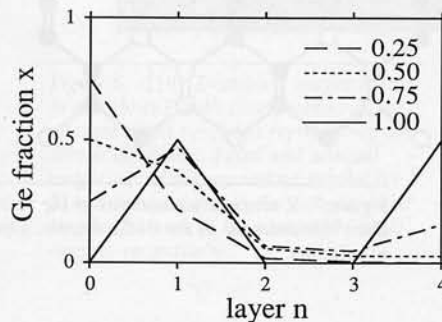


Figure 10. Ge fraction x for alloy columns in the n -th deposited Si layer of a $(Si_xGe_x)_p$ superlattice as a function of the atom pump parameter α (see text).

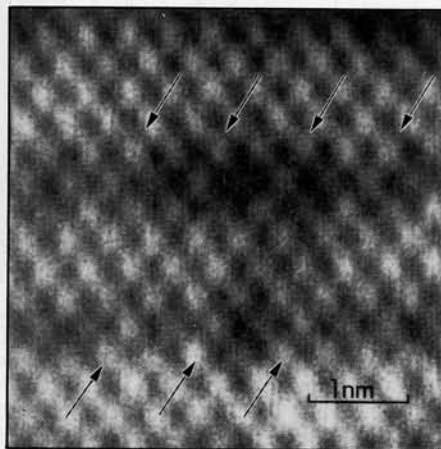


Figure 11. Z-contrast image of part of a $(Si_4Ge_8)_{24}$ superlattice exhibiting an antiphase boundary of the ordered superlattice.

tion which we set out to answer ("which is the true ordered phase?") becomes totally inappropriate for low-temperature growth. We must rather think of many possible phase variants arising as a natural consequence of growth-induced compositional ordering.

We can even proceed a stage further in our analysis if we consider the Ge concentration gradient explicitly. Defining an adatom-substrate exchange parameter α (i.e., a "pumping" parameter) as the fraction of available Ge atoms which are pumped during each growth step, we can generate Z-contrast image simulations of the ordered phases. We find excellent agreement between the simulations and experiment for $\alpha \approx 0.75$ (Figure 8) and can deduce a model for precisely how the superlattice has grown in this region. Assuming α has the usual Arrhenius temperature dependence, we can predict how the growth temperature will affect the pump mechanism and hence the superlattice microstructure.

Figure 10 summarizes this behavior, showing the pumped Ge concentration in the Si layers of a $(Si_xGe_x)_p$ superlattice. Low temperatures (small α) favor the growth of abrupt interfaces, which lends support to the strategy suggested by Iyer et al.¹⁴ involving deposition at around 250°C followed by rapid thermal annealing. Intermediate temperatures (300–400°C) will involve strong ordering as observed experimentally. Notice the buildup of pumped Ge in the fourth Si layer which is trapped as the low-energy Ge surface is deposited in the fifth layer. The fourth layer Ge concentration is, however, significantly smaller than the first layer concentration which is the origin of the asymmetric interfacial abruptness observed in our images. Our model, therefore, provides a clear atomistic picture of the well-known effect of Ge segregation during MBE growth¹⁴ and also links the effect with $\langle 111 \rangle$ ordering.

To obtain abrupt interfaces in this important temperature regime, it would seem necessary to modify the surface growth dynamics, for example, by utilizing a suitable surfactant (surface active species).^{15,16} Although at present the exact growth modes are unclear, it would seem that a species such as As serves to passivate the surface dangling bonds, thus removing the driving force for the pump mechanism.

We also observe defects in the ordering as illustrated in Figure 11. In the lower Si layer, we have $\langle 111 \rangle$ planar ordering of alloy dumbbells which are indicated by the arrows. The pump mechanism is extinguished as the Ge

layers are deposited but restarts as the next Si layer is grown. Again, by statistical chance, we obtain $\langle 111 \rangle$ planar ordering but notice that the bright stripes are now out of phase with the bright stripes in the lower Si layer. Hence, we have an antiphase domain boundary of the ordered superlattice. Such defects are entirely consistent and indeed would be expected from our growth model. The translations will, however, invariably complicate the interpretation of spot intensities in diffraction patterns.

It is important that clear projections of the ordered structures are visible only in the thinnest regions of specimens. This would be expected from the intrinsically small domain size discussed earlier so that in thicker samples, the overlap of several domains in projection gives the impression of diffuse interfaces. The ability of Z-contrast STEM to image intuitively over a wide range of specimen thickness is, therefore, a significant advantage.

The fact that all the experimental features in Figure 8 can be explained by our growth model lends strong support to the pump mechanism which was derived from relatively simple considerations of bonding energetics. We emphasize, however, that the insights provided by Z-contrast STEM present a unique opportunity for focused theoretical studies such as total energy minimization calculations applied to steps. In this way, it should be possible to gain a deeper understanding of the fundamental atomistic processes occurring during MBE growth.

Our second example of the insight provided by intuitive imaging concerns the interface between epitaxial CoSi_2 and $\text{Si}(100)$ shown in Figure 12. This interface is generally assumed to be flat and possibly reconstructed over extended regions (see the article by J.M. Gibson in this issue). The Z-contrast image of the CoSi_2 is dominated by strongly scattering Co columns which display an apparent $(4 \times n)$ compositional ordering at the interface plane. This periodicity is only observed to extend over small regions and does not show up in diffraction studies. Rather than representing an intrinsic interfacial reconstruction, it seems more likely that these structures reflect the preservation of interface defects during growth.

The interface shown in Figure 12 was grown by the template method¹⁷ in which Co is initially deposited at elevated temperatures to react with the first few monolayers of a Si surface to produce a silicide template layer for subsequent CoSi_2 growth. It is well known

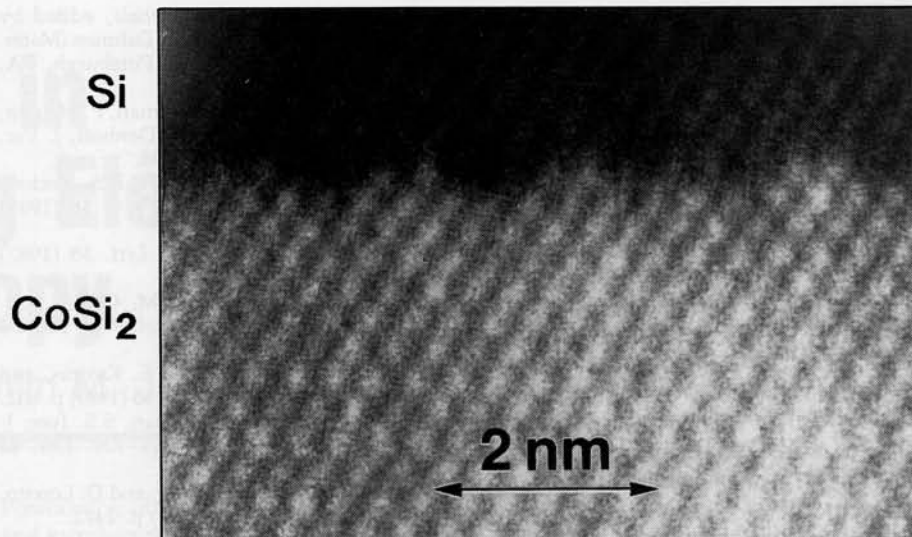


Figure 12. Z-contrast image of interfacial defects at an epitaxial $\text{CoSi}_2/\text{Si}(100)$ interface.

from STM that, after cleaning, the original Si surface contains various dimer row defects¹⁸ which could well be preserved during the chemical reaction, as suggested by Figure 12. These observations are very important because the electrical properties of such defects are entirely unknown and could well be affecting the measured height of the Schottky barrier. Thus again, insight is provided by the powerful combination of STM and STEM, which will undoubtedly play an increasingly important role in future studies of epitaxial growth.

Conclusions

The chief advantage of Z-contrast STEM in the study of semiconductor interfaces is that it is truly a direct imaging technique. Each interface can have only one possible image so that interfacial structure and chemistry can be deduced directly from the image. This unique ability has already enabled us to observe unexpected phenomena in systems studied for many years using various techniques. It is becoming increasingly apparent that surface growth dynamics can influence the final atomic arrangements in quite subtle but important ways. STM combined with Z-contrast STEM therefore represents an exciting opportunity to understand the fundamental atomistic processes which occur during epitaxial growth and their role in determining the final microstructure.

The current development of a 300 keV STEM with an anticipated 1.4 Å probe

size will extend the Z-contrast technique to provide sublattice sensitivity in semiconductor materials along several major zone axes. Combined with column-by-column spectroscopic analysis using localized inelastic excitations, microdiffraction, and phase contrast chemical mapping techniques, the methods of analytical and high-resolution electron microscopy could finally merge on the same instrument, providing a completely new level of characterization for the study of materials of all kinds.

Acknowledgments

It is a pleasure to thank M.F. Chisholm for useful discussions, J.-M. Baribeau, and D.C. Houghton for providing the ultrathin Si-Ge superlattices, S.M. Yalisove and R.T. Tung for providing the CoSi_2 film, and T.C. Estes, J.T. Luck, and S.L. Carney for technical assistance. This research was sponsored by the Division of Materials Sciences, U.S. Department of Energy, under contract DE-AC05-84OR21400 with Martin Marietta Energy Systems, Inc., and in part by an appointment to the U.S. Department of Energy Postgraduate Research Program at ORNL administered by Oak Ridge Associated Universities.

References

1. See, for example, A. Ourmazd, *MRS Bulletin* 15 (9) (1990) p. 64; errata 15 (11) (1990) p. 18.
2. S.J. Pennycook and D.E. Jesson, *Phys. Rev. Lett.* 64 (1990) p. 938.